International Journal of Heat and Mass Transfer 92 (2016) 1041–1052

Contents lists available at ScienceDirect

International Journal of Heat and Mass Transfer

journal homepage: www.elsevier.com/locate/ijhmt

Experimental and numerical investigation of nanofluids heat transfer characteristics for application in solar heat exchangers

Ehsan Ebrahimnia-Bajestan [a], Mohammad Charjouei Moghadam [b], Hamid Niazmand [b,*], Weerapun Daungthongsuk [c], Somchai Wongwises [c]

[a] Department of Energy, Institute of Science and High Technology and Environmental Science, Graduate University of Advanced Technology, Kerman, Iran
[b] Department of Mechanical Engineering, Ferdowsi University of Mashhad, Mashhad, Iran
[c] Fluid Mechanics, Thermal Engineering and Multiphase Flow Research Laboratory (FUTURE), Department of Mechanical Engineering, Faculty of Engineering, King Mongkut's University of Technology Thonburi, Bangmod, Bangkok, Thailand

ARTICLE INFO

Article history:
Received 6 July 2015
Received in revised form 9 August 2015
Accepted 10 August 2015

Keywords:
Nanofluid
Convective heat transfer
Experimental study
Two-phase modeling
Solar systems

ABSTRACT

One of the innovative methods of improving heat transfer characteristics of heat exchangers in solar systems is applying nanofluids as the heat transfer media. In this study, laminar convective heat transfer of water-based TiO_2 nanofluid flowing through a uniformly heated tube has been investigated via experiments and numerical modeling. The thermal conductivity and dynamic viscosity of the prepared nanofluids have also been measured and modeled at different temperatures and nanoparticle concentrations. Based on the results, a maximum enhancement of 21% in average heat transfer coefficient has been obtained using TiO_2/water nanofluids. For the numerical section, the single-phase model was compared with the common two-phase numerical approaches. The numerical investigation indicated that the predicted heat transfer coefficients using single-phase and common two-phase approaches, even based on experimental thermophysical properties of nanofluids, underestimate and overestimate the experimental data, respectively. Therefore, some modifications are implemented to the common two-phase model in order to obtain more accurate predictions of the heat transfer characteristics of nanofluids. This modified model investigated the effects of particle concentration, particle diameter, and particle and basefluid material on the heat transfer rate at different Reynolds numbers. The results indicated that the convective heat transfer coefficient increases with an increase in nanoparticle concentration and flow Reynolds number, while particle size has an inverse effect. The obtained results can be very useful to the investigation of the potential application of nanofluid-based solar collectors.

1. Introduction

A solar-liquid heating collector transforms the solar energy to the internal energy of the transport medium as a kind of heat exchanger. The performance of these heat exchangers can be enhanced by improving thermophysical properties of the conventional heat transfer fluids. Recently, nanofluids have attracted great interest due to their valuable heat transfer characteristics in comparison with conventional fluids.

Several researchers [1–9] have investigated the application of these new media of heat transfer in solar collectors. Yousefi et al. [1] experimentally revealed that the Al_2O_3/water nanofluid enhances the efficiency of flat-plate collectors by 28.3%. In another study, Yousefi et al. [2] examined the effects of pH values of carbon nanotube nanofluids on the efficiency of a flat-plate solar collector. Kameya and Hanamura [3] demonstrated that the radiation absorption characteristics of base fluid were enhanced dramatically by adding Ni nanoparticles. Lenert and Wang [4] examined the capability of nanofluids as volumetric receivers in concentrated solar applications using the suspension of carbon-coated cobalt nanoparticles into Therminol VP-1 fluid. He et al. [5] experimentally expressed the suitable photo-thermal properties of Cu/H_2O nanofluids for employment in direct absorption, solar thermal energy systems.

Moreover, the recent review papers [10,11] indicated that nanofluids have great potential for applications in solar systems such as solar collectors [12], photovoltaic thermal systems [13], and thermal energy storage systems [14].

* Corresponding author.
E-mail addresses: ehsan.ebrahimnia@gmail.com (E. Ebrahimnia-Bajestan), Niazmand@um.ac.ir (H. Niazmand), somchai.won@kmutt.ac.th (S. Wongwises).

http://dx.doi.org/10.1016/j.ijheatmasstransfer.2015.08.107
0017-9310/

Nomenclature

A	cross sectional area, m^2
c_p	specific heat, J/(kg K)
d_p	particle diameter, m
D_{pipe}	pipe diameter, m
h	heat transfer coefficient, W/(m^2 K)
k	thermal conductivity, W/(m K)
l_p	nanotube length, m
L_{pipe}	pipe length, m
Nu	Nusselt number, hD_{pipe}/k_e
p	pressure, Pa
q''	heat flux, W/m^2
R	electrical resistance, Ω
Re_e	Reynolds number, $\rho_e U_{in} D_{pipe}/\mu_e$
t	time, s
T	temperature, K
v	velocity vector, m/s
V	phase volume, m^3
V_{in}	inlet voltage to the Wheatstone bridge, V

Greek Symbols

ρ	density, kg/m^3
μ	dynamic viscosity, kg/(m s)
φ	volume concentration
κ	Boltzmann constant, 1.381×10^{-23} J/K

Subscripts

e	effective properties of nanofluid
f	base fluid
i	phase i
p	nanoparticle
w	wall

Table 1
Literature review on the experimental study of laminar convective heat transfer of nanofluids in the straight tubes.

Investigator(s)	Particle type	Particle shape	Particle concentration	Geom. L_{pipe}/D_{pipe}	Boundary condition	Enh. of h	Classical correlation ability
Li and Xuan [18]	Cu	d_p < 100 nm	0.3–2 vol.%	80	q'' = Const.	60%	x
Wen and Ding [19]	Al_2O_3	d_p < 27–56 nm	0.6–1.6 vol.%	215	q'' = Const.	30%	x
Ding et al. [20]	CNT	d_p < 100 nm l_p>> 100 nm	0.1–0.5 wt.%	215	q'' = Const.	300%	x
Heris et al. [21]	Al_2O_3 CuO	d_p = 20 nm d_p = 50–60 nm	0.2–3 vol.%	167	T_w = Const.	–	x
He et al. [22]	TiO_2	d_p = 95 nm	0.2–1.2 vol.%	483	q'' = Const.	26%	x
Chen et al. [23]	TNT	d_p = 10 nm l_p = 100 nm	0.5–1.5 wt.%	483	q'' = Const.	25%	–
Hwang et al. [24]	Al_2O_3	d_p = 30 nm	0.01–0.3 vol.%	1380	q'' = Const.	8%	x
Lai et al. [25]	Al_2O_3	d_p = 20 nm	0.5–1 vol.%	490	q'' = Const.	55%	x
Anoop et al. [26]	Al_2O_3	d_p = 45, 150 nm	1–4 wt.%	250	q'' = Const.	13%	–
Heris et al. [27]	Cu	d_p = 25 nm	0.2–2.5 vol.%	167	T_w = Const.	45%	x
Rea et al. [28]	Al_2O_3 ZrO_2	d_p = 50 nm	0.65–6 vol.% 0.32–1.32 vol.%	244	q'' = Const.	22% 3%	OK
Liao and Liu [29]	CNT	d_p = 10–20 nm l_p = 1–2 μm	0.5–2 wt.%	217	q'' = Const.	60%	x
Kim et al. [30]	Al_2O_3 C	d_p = 20 nm	3 vol.% 3.5 vol.%	437	q'' = Const.	20% 8%	–
Asirvatham et al. [31]	Ag	d_p < 100 nm	0.3–0.9 vol.%	683	T_w = Const.	150%	–
Chandrasekar and Suresh [32]	Al_2O_3	d_p = 43 nm	0.1–0.2 vol.%	247	q'' = Const.	60%	–
Ferrouillat et al. [33]	SiO_2	d_p = 22 nm	2.3–19 vol.%	50	T_w = Const.	–	OK
Kumaresan et al. [34]	CNT	d_p < 100 nm	0.15%–0.45 vol.%	233	–	125%	x
Rayatzadeh et al. [35]	TiO_2	–	0.1–0.025 vol.%	652	q'' = Const.	65%	–
Esmaeilzadeh et al. [36]	Al_2O_3	d_p = 15 nm	0.5–1 vol.%	143	q'' = Const.	19%	–
Heyhat et al. [37]	Al_2O_3	d_p = 40 nm	0.1–2 vol.%	400	T_w = Const.	32%	x
Wang et al. [38]	CNT	d_p = 20–30 nm l_p = 5–30 μm	0.05–0.24 vol.%	1000	q'' = Const.	190%	x

X: Classical correlations fail to predict convective heat transfer of nanofluids.
OK: Classical correlation succeed to predict convective heat transfer of nanofluids.

Most of the investigations on the application of nanofluids in solar collectors have been limited to energy and exergy analysis. There are few studies on the analysis of the hydrodynamic and convective heat transfer characteristics of nanofluids in solar systems [6].

As highlighted in several review papers [15–17], a substantial amount of experimental work has been reported on the thermal behavior of different types of nanofluids flowing through various heat exchanger geometries; among them, the circular straight tubes have received more attention in this study since they are the main component of different types of solar collectors. In this geometry, a variety of nanoparticle types and concentration levels under various thermal boundary conditions have been examined, which are listed in Table 1. This table reports the ratio of tube length to the tube diameter (L_{pipe}/D_{pipe}) and the amount of heat transfer coefficient enhancement due to the use of nanofluids. Furthermore, the ability of classical models for predicting the heat transfer coefficient of nanofluid flow through the tubes is determined.

It is evident from Table 1 that nearly all researchers have reported that the classical correlations, such as those mentioned by Shah and London [39], are incapable of predicting the superior convective heat transfer characteristics of nanofluids, which demonstrates the need for remodeling of the nanofluids heat transfer.

As for numerical modeling, numerous researchers [40,41] have adopted the single-phase approach for the simulation of

laminar convective heat transfer of nanofluids in straight pipes. Ebrahimnia-Bajestan et al. [40] showed that measuring temperature-dependent properties of nanofluids at static condition and employing them in a single-phase approach is not sufficient to predict the convective heat transfer characteristics of nanofluids accurately, and thermophysical properties should be modified based on the dynamic condition.

Several studies [42–46] compared the ability of both two-phase and single-phase approaches in predicting the laminar convective heat transfer of nanofluid flow in the straight tube. In general, two-phase models, such as mixture and Eulerian–Eulerian, give more accurate heat transfer results compared with the single-phase approaches; yet, the relative errors are still significant (i.e., more than 10%). Furthermore, most of the available investigations [47–50] on the mixture and Eulerian–Eulerian models have not been validated against the experimental data. The few available studies [51,52] that have reported reasonable agreement between mentioned two-phase models and measured data, have just considered cases of very low nanoparticle concentrations (lower than 1 vol.%).

The main drawback of mixture and Eulerian–Eulerian models is the fact that they commonly use predefined correlations that have been developed for millimeter- or micrometer-sized particles. Therefore, the surface interaction effects of nano-systems are not properly considered, which causes the relative errors of the heat transfer predictions to be more than 10% in some cases.

Considering the above, there are still many challenges regarding the application of nanofluids in solar-systems heat exchangers, which indicates the crucial need for more investigations in the field of convective heat transfer of nanofluids.

The present study investigates the laminar convective heat transfer of TiO_2/water nanofluid in a straight tube both experimentally and numerically. Focusing on the the straight tube as the main part of different kinds of solar collectors, such as flat plate and parabolic trough collectors, can be very useful to the investigation of the potential application of nanofluid-based solar collectors. Considering Table 1, few studies are conducted on the laminar convective heat transfer of theTiO_2 nanofluids. Titanium dioxide is chosen as the nanoparticle due to its excellent chemical and physical stabilities. It is also commercially available and regarded as a safe material.

Moreover, thermal conductivity and viscosity of the TiO_2/water nanofluid are measured for employing in the single-phase model. In the case of a two-phase approach, Eulerian–Eulerian and mixture models are applied. In addition, a modified correlation of the Eulerian–Eulerian model has been proposed for the calculation of the heat exchange between the nanoparticle and base fluid, where its accuracy is evaluated based on the measured data. Furthermore, the effects of other parameters, such as particle diameter and concentration, as well as particle and base fluid material on the heat transfer coefficient are investigated using the modified model.

2. Experimental method and equipment

2.1. Sample preparation

The employed nanofluid consists of DEGUSSA P25 TiO_2 nanoparticles with a mean diameter of 21 nm dispersed into deionized water. In order to prepare the nanofluid at a certain concentration, the cetyl trimethyl ammonium bromide (CTAB) at very low concentration (about 0.1 mM) was solved into water. Then, inside an ultrasonic bath (600 W, 40 kHz), the nanoparticles were added to the solution little by little and simultaneously sonicated continuously for approximately 3–5 h to break down the nanoparticles agglomerations and manufacture a homogenous and stable mixture. The stable suspensions were provided at different nanoparticles volume concentrations of 1, 1.5, 1.6, 2, and 2.3% without visually observable sedimentation for the duration of about 3 months.

2.2. Experimental apparatus

2.2.1. Thermophysical properties measurements

The study employed a Cannon–Fenske Opaque (Reverse-Flow) viscometer placed inside a heat exchanger to measure the viscosity of the prepared nanofluids at different particle concentrations and temperatures. The experimental apparatus for viscosity measurement is shown schematically in Fig. 1. It should be mentioned that a survey of literature data [53–55] shows that the TiO_2/water nanofluid exhibits a Newtonian behavior at low particle concentrations employed in this study. Therefore the mentioned viscometer is proper to measure the viscosity of the prepared nanofluids.

In order to measure the thermal conductivity of the nanofluids, an apparatus based on the hot wire technique (Fig. 2) was designed and built as presented in detail in Duangthongsuk and Wongwises [56]. The main part of this apparatus is the Wheatstone bridge, in which $R_2 = 22\ k\Omega$ and $R_3 = 10\ \Omega$, where the R_1 is a 22 k Ω variable resistor to balance the Wheatstone bridge circuit. A voltage source of $V_{in} = 7$ V provided by a DC power supply was applied to the bridge. The resistance of R_w represents the platinum hot wire of 50 μm in diameter and 19 cm in length that was insulated with a Teflon layer of 25 μm. In this technique, the platinum wire was employed as the line heat source and temperature sensor, since the relation between its resistance and temperature is known over a wide temperature range.

The platinum wire was installed in the center line of a container full of nanofluid and of sufficiently large diameter in comparison with the diameter of platinum wire. This container was placed inside

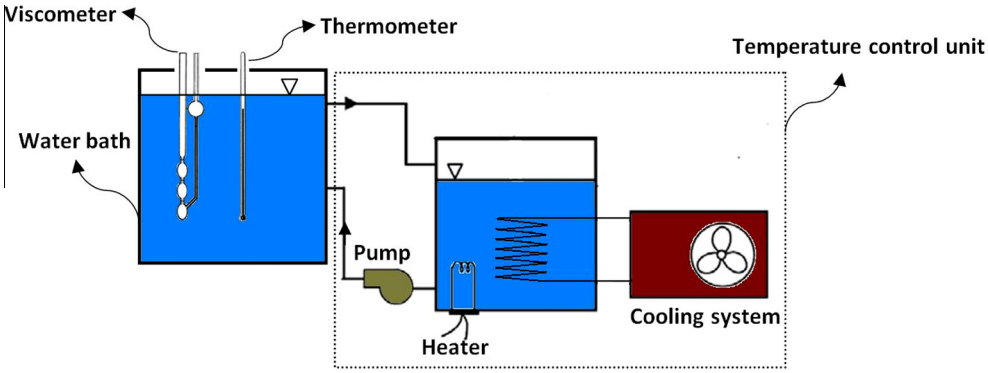

Fig. 1. Schematic diagram of the viscosity measurement at different temperature.

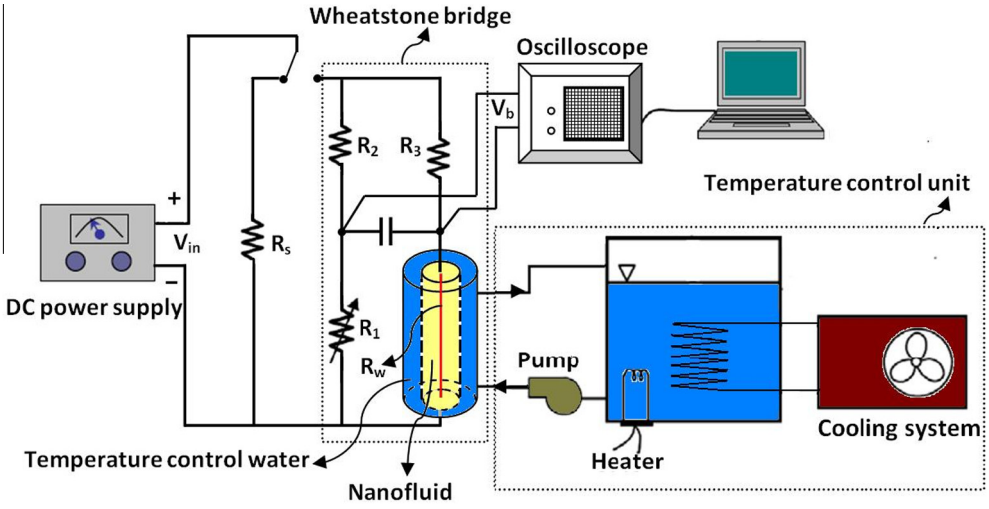

Fig. 2. Schematic diagram of transient hot water technique for viscosity measurement at different temperature.

a bigger container filled with circulating water provided by a thermostatic bath to keep the nanofluid temperature at the desired value. Finally, the thermal conductivity of the nanofluids was calculated from the equation $k_e = \frac{q}{4\pi(T_2-T_1)} \ln\left(\frac{t_1}{t_2}\right)$, where k_e is the thermal conductivity, q is the applied electric power per unit length of the wire, and $T_2 - T_1$ is the temperature rise of the wire between time t_1 and t_2.

2.2.2. Convective heat transfer apparatus

The schematic of the experimental apparatus for the study of laminar convective heat transfer of the nanofluid is shown in Fig. 3. The test section is a 2 m long, horizontal, straight copper tube with a 7.8 mm inner diameter and 9.6 mm outer diameter. The tube was heated by a flexible silicon rubber heater of 313 W (BriskHeat® Corporation) that was linked to a DC power supply. To obtain a constant and uniform heat flux condition along the test section, the heater was wrapped in 5 layers of thermal insulating materials, and to further minimize the heat loss, it was covered with a 2 cm thick foam insulation layer. In order to measure the wall temperature, 10 T-type thermocouples (with the precision of ±0.1 °C) were mounted along the surface of the test section and 2 further T-type thermocouples were inserted into the flow at the inlet and outlet of the test section to measure the bulk temperatures of nanofluids. Two sight glass tubes with an inner diameter equal to the test section were installed before and after the test section to visualize the nanofluid flow and probable nanoparticles sedimentation. The nanofluid flow rate was controlled by adjusting the rotation speed of the magnetic gear pump and measured by the weighing method.

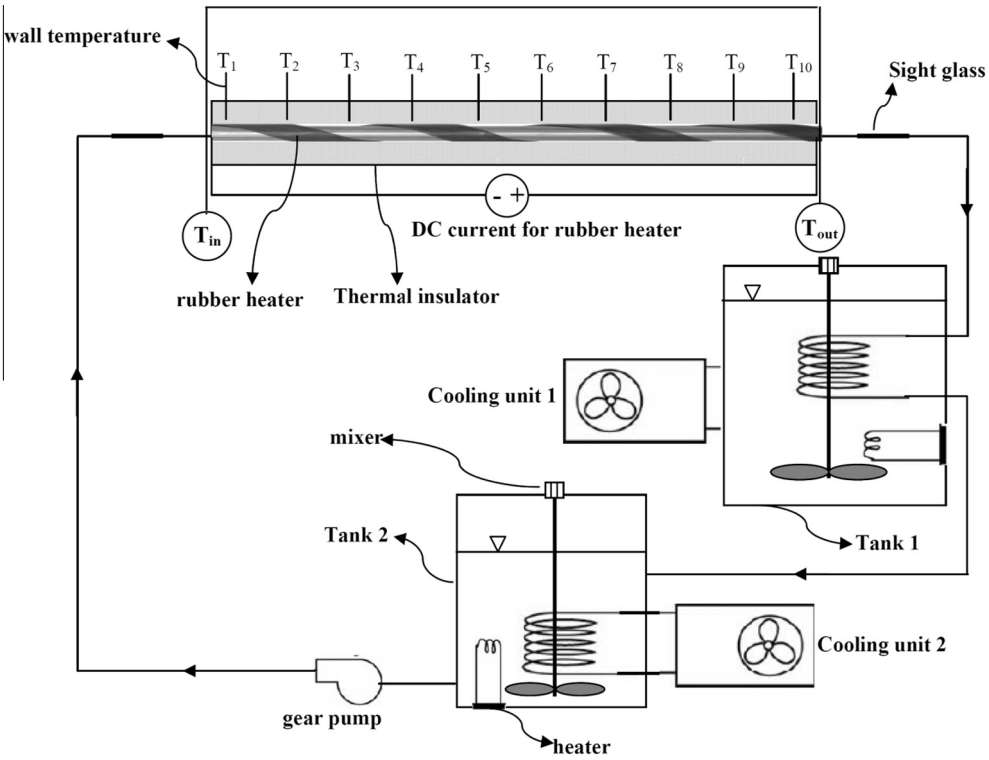

Fig. 3. Schematic diagram of the experimental apparatus.

2.2.3. Uncertainties

The uncertainties of the measured data were calculated based on the uncertainty of the test equipment S_d, and the uncertainty due to repeatability S_r, as follows.

$$S_t = \sqrt{S_d + S_r} \tag{1}$$

The uncertainty due to repeatability is equal to the standard deviation of the sample data, which is given by Eq. (2) for the quantity of q_t.

$$S_{r,q} = \sqrt{\frac{1}{m-1}\sum_{j=1}^{m}(q_{t_j} - \overline{q_t})^2} \tag{2}$$

where q_{t_j} is the jth reading of sample, and $\overline{q_t}$ is the mean value of the m samples, which is computed from Eq. (3).

$$\overline{q_t} = \frac{1}{m}\sum_{j=1}^{m} q_{t_j} \tag{3}$$

In the case of equipment and devices uncertainties, if the variables were measured directly by the instrument, such as viscosity, the uncertainty of that instrument was used. However, if a quantity was computed from measurements of two or more parameters, a mathematical relationship was necessary between the quantity and the measured variables parameters. If this equation is expressed as $q_t = f(x,y,z,\ldots)$ where q_t is the quantity and x, y, z,... are the measured variables parameters, the uncertainty of q_t is as follows.

$$S_{d,q} = \delta q_t = \sqrt{\left(\frac{\partial q_t}{\partial x}\delta x\right)^2 + \left(\frac{\partial q_t}{\partial y}\delta y\right)^2 + \left(\frac{\partial q_t}{\partial z}\delta z\right)^2 + \cdots} \tag{4}$$

Based on the mentioned method, the computed uncertainties for the thermal conductivity, viscosity, and average heat transfer coefficient were found to be about 0.00899 W/m K (1.3%), 9.34×10^{-6} Pa.s (0.88%), and 14.5 W/m^2 K (2.8%), respectively.

3. Numerical modeling

3.1. Grid-independence study

In order to find the minimum grid points needed to produce reasonably grid-independent results, extensive computations were performed. The variations of the Nusselt number along the tube are shown in Fig. 4 for a 2.3 vol.% TiO_2/water nanofluid at different grid structures. The study found that in total, 1460 computational cells are required for the circular cross section of the tube while 205 grid points are needed in the axial direction. The meshes are denser near the tube wall.

3.2. Single-phase modeling

For an incompressible, steady-state flow, the governing equations, as well as the thermophysical properties of the nanofluid, are as follows:

Continuity equation:

$$\nabla \cdot (\rho_e \vec{v}) = 0 \tag{5}$$

Momentum equation:

$$\nabla \cdot (\rho_e \vec{v}\vec{v}) = -\nabla p + \nabla.(\mu_e \nabla \vec{v}) \tag{6}$$

Energy equation:

$$\nabla \cdot (\vec{v}(\rho c_p)_e T) = \nabla \cdot (k_e \nabla T) \tag{7}$$

Density:

$$\rho_e(\varphi, T) = (1-\varphi_p)\rho_f(T) + \varphi_p \rho_p \tag{8}$$

Heat capacity:

$$c_{p,e}(\varphi, T) = \frac{(1-\varphi_p)(\rho(T)C_p(T))_f + \varphi_p(\rho c_p)_p}{(1-\varphi_p)\rho_f(T) + \varphi_p \rho_p} \tag{9}$$

Fig. 5 presents the dynamic viscosity of the TiO_2/water nanofluid that was measured at different particle concentrations and temperatures. The results indicate that the nanofluid viscosity strongly decreases as temperature increases. The observed viscosity increase due to the increase in particle concentration can be attributed to the high surface-area-to-volume ratio of the nanoparticles, which increases the resistance of fluid flowing.

The dynamic viscosity of the TiO_2/water nanofluid was modeled based on the presently measured data, employing a semi-empirical expression proposed by Koo and Kleinstreuer [57] as expressed by Eq. (10). The correlations (10c) and (10d) were obtained from a curve fitting on the measured data of this study. Fig. 5 displays the comparison of the measured data and the predicted results from the Eq. (10).

$$\mu_e = \mu_{static} + \mu_{Brownian} \tag{10}$$

$$\mu_{static} = (1 + 2.5\varphi_p)\mu_f \tag{10a}$$

$$\mu_{Brownian} = 5 \times 10^4 \beta \rho_f \varphi_p \sqrt{\frac{\kappa T}{\rho_p d_p}} f(\varphi, T) \tag{10b}$$

$$\beta = 0.0000308 \times (100\varphi_p)^2 - 0.0000287 \times (100\varphi_p) + 0.000834 \tag{10c}$$

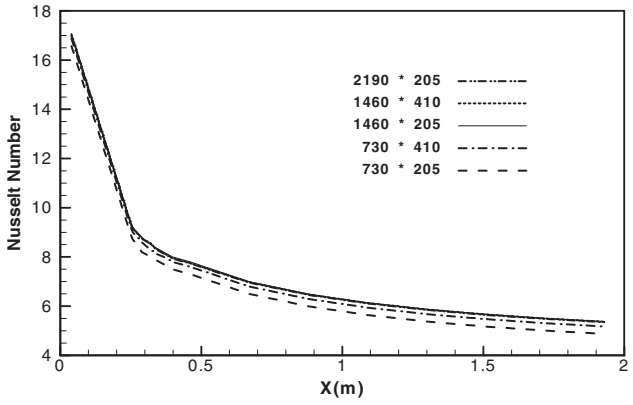

Fig. 4. Model grid independency check for 2.3 vol.% TiO_2/Water nanofluid at Reynolds number of 935.

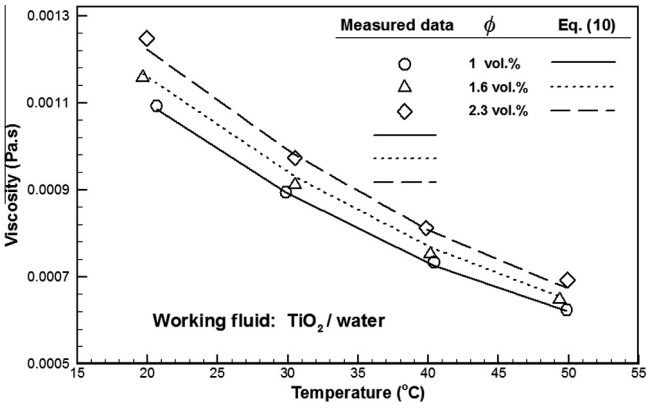

Fig. 5. Measured data and predicted values of viscosity for the TiO_2/water nanofluid at different particle concentrations and temperatures.

$$f(\varphi,T) = (-0.4602 + 1.217\varphi_p)(T - 273.15) + (45.16 - 522.8\varphi_p) \quad (10d)$$

Moreover, the measured data of the thermal conductivity of the nanofluid is shown in Fig. 6 for different particle concentrations and temperatures. Clearly, the thermal conductivity of the TiO_2/water nanofluid is higher than that of water even at low particle concentrations. This is due to (a) the higher thermal conductivity of TiO_2 nanoparticles in comparison with water, (b) the Brownian motion of nanoparticles into the base fluid, and (c) bulk motion due to the Brownian motion of nanoparticles that results in a strong fluid-mixing and heat transfer enhancement. Again, the semi-empirical expression proposed by Koo and Kleinstreuer [57] was employed to correlate the presently measured data as expressed by Eqs. (11)–(11d). The correlations (11c) and (11d) were obtained from a curve fitting on the measured data of this study. It should be mentioned that in these equations, all thermophysical properties of the base fluid are temperature dependent. The comparison of the measured data and the predicted results from Eq. (11) is depicted in Fig. 6.

$$k_e = k_{static} + k_{brownian} \quad (11)$$

$$k_{static} = \frac{k_p + 2k_f + 2\varphi_p(k_p - k_f)}{k_p + 2k_f - \varphi_p(k_p - k_f)} k_f \quad (11a)$$

$$k_{brownian} = 5 \times 10^4 \beta (\rho c_p)_f \varphi_p \sqrt{\frac{\kappa T}{\rho_p d_p}} f(\varphi,T) \quad (11b)$$

$$\beta = 0.000867 \times (100\varphi_p)^{-0.9475} \quad (11c)$$

$$f(\varphi,T) = (-0.4527\varphi_p - 0.02295)(T) + (128.1\varphi_p + 7.883) \quad (11d)$$

In the aforementioned equations, temperature-dependent thermophysical properties of water were obtained from the curve fitting to the data of ASHRAE Handbook [58]. The same attempt was performed for the ethylene glycol to water mixture (60:40 by mass), which is considered another base fluid in this study.

- Thermophysical properties of water

$$\rho_f = -0.003T^2 + 1.505T + 816.781 \quad (12)$$

$$c_{p,f} = -0.0000463T^3 + 0.0552T^2 - 20.86T + 6719.637 \quad (13)$$

$$k_f = -7.843 \times 10^{-6}T^2 + 0.0062T - 0.54 \quad (14)$$

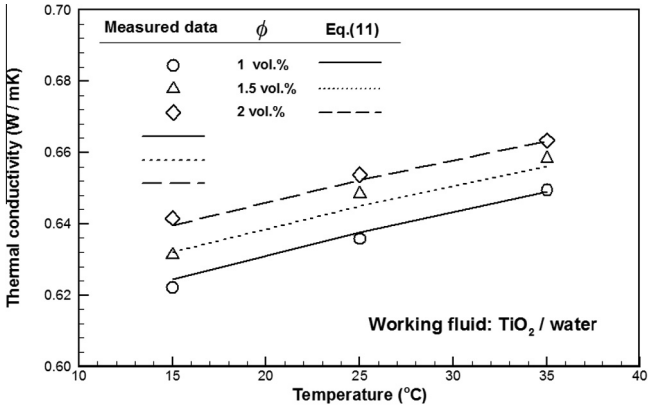

Fig. 6. Measured data and predicted values of thermal conductivity for the TiO_2/water nanofluid at different particle concentration and temperature values.

$$\mu_f = 0.00002414 \times 10^{(247.8/(T-140))} \quad (15)$$

- Thermophysical properties of ethylene glycol to water mixture (EG:W)

$$\rho_f = -0.002475T^2 + 0.9998T + 1002.5 \quad (16)$$

$$c_{p,f} = 4.248T + 1882.4 \quad (17)$$

$$k_f = -3.196 \times 10^{-6}T^2 + 0.0025T - 0.1054 \quad (18)$$

$$\mu_f = 0.001 \times exp\left(3135.6 \times \frac{1}{T} - 8.9367\right) \quad (19)$$

In addition, the thermophysical properties of different nanoparticles assumed to be temperature independent have been listed in Table 2.

The governing equations were solved numerically using the control-volume method by the commercial FLUENT 6.3 software. In this study, all thermophysical properties of nanofluids and base fluids, based on the above equations, were incorporated into the main solver by developing several user defined functions (UDFs) in C language.

3.3. Two-phase modeling

3.3.1. Eulerian–Eulerian model

In the Eulerian–Eulerian model, an Eulerian treatment is used for each phase of nanoparticle and base fluid, where momentum and continuity equations are solved for each phase separately. The same pressure field is shared by both phases. The related governing equations for the steady-state laminar flow are as follows:

The volume of phase i, V_i is defined by

$$V_i = \int \varphi_i dV \quad (20)$$

For the volume concentration of base fluid and particle phases,

$$\varphi_f + \varphi_p = 1 \quad (21)$$

Continuity equation for different phases of $i = f$ and p:

$$\nabla \cdot (\varphi_i \rho_i \vec{v}_i) = 0 \quad (22)$$

Momentum equation for 2 phases,

$$\nabla \cdot (\varphi_f \rho_f \vec{v}_f \vec{v}_f) = -\varphi_f \nabla p + \nabla \cdot \bar{\bar{\tau}}_f + \vec{R}_{pf} \quad (23)$$

$$\nabla \cdot (\varphi_p \rho_p \vec{v}_p \vec{v}_p) = -\varphi_p \nabla p + \nabla \cdot \bar{\bar{\tau}}_p - \vec{R}_{pf} \quad (24)$$

where $\bar{\bar{\tau}}_i$ is the i^{th} phase stress–strain tensor,

$$\bar{\bar{\tau}}_i = \varphi_i \mu_i \nabla \vec{v}_i \quad (25)$$

$\vec{R}_{pf}$ is the interaction force between the base fluid and particle phases. This force depends on the friction, pressure, cohesion, and other effects. FLUENT uses a simple interaction term of the following form [59]:

$$\vec{R}_{pf} = K_{pf}(\vec{v}_p - \vec{v}_f) \quad (26)$$

Table 2
Thermophysical properties of nanoparticles.

Particles	ρ (kg/m^3)	C_p (J/kgK)	k (W/mK)
TiO_2	4157	710	8.4
Al_2O_3	3970	765	40
CuO	6350	535.6	76.5

K_{pf} is the interphase momentum exchange coefficient, which can be written in the following general form:

$$K_{pf} = (\varphi_f \varphi_p \rho_p C_D \mathrm{Re}_p)/(24\tau_p) \tag{27}$$

where particulate relaxation time is defined as

$$\tau_p = \rho_p d_p^2/18\mu_f \tag{28}$$

Here, C_D is the drag coefficient obtained from the Schiller and Naumann model [60].

$$C_D = \begin{cases} \frac{24(1+0.15\,\mathrm{Re}_p^{0.687})}{\mathrm{Re}_p}, & x < 0 \\ 0.44, & x \geqslant 0 \end{cases} \tag{29}$$

in which, the relative Reynolds number is defined as

$$\mathrm{Re}_p = \frac{\rho_f |\vec{v}_p - \vec{v}_f| d_p}{\mu_f} \tag{30}$$

To describe the conservation of energy in Eulerian multiphase applications, a separate enthalpy equation can be written for each phase.

$$\nabla \cdot (\varphi_f \rho_f h_f \vec{v}_f) = \bar{\bar{\tau}}_f : \nabla \vec{v}_f - \nabla \cdot \vec{q}_f - Q_{pf} \tag{31}$$

$$\nabla \cdot (\varphi_p \rho_p h_p \vec{v}_p) = \bar{\bar{\tau}}_p : \nabla \vec{v}_p - \nabla \cdot \vec{q}_p + Q_{pf} \tag{32}$$

where h_i and $\vec{q}_i$ are specific enthalpy and heat flux of the i^{th} phase, respectively. Q_{pf} is the intensity of heat exchange between the base fluid and nanoparticle phases.

$$Q_{pf} = h_V (T_f - T_p) \tag{33}$$

in which h_V is the volumetric heat transfer coefficient between the nanoparticles and the base fluid.

$$h_V = \frac{(6k_f \varphi_p \varphi_f \mathrm{Nu}_p)}{d_p^2} \tag{34}$$

The heat transfer coefficient is related to the nanoparticle Nusselt number, $\mathrm{Nu_p}$, which is determined from the Ranz-Marshall correlation [61],

$$\mathrm{Nu}_p = 2 + 0.6\mathrm{Re}_p^{0.5}\mathrm{Pr}_f^{1/3} \tag{35}$$

where Pr_f is the base fluid Prandtl number,

$$\mathrm{Pr}_f = \frac{C_{p,f}\mu_f}{k_f} \tag{36}$$

3.3.2. Modifications to the Eulerian–Eulerian model

As mentioned earlier, the above procedure for the prediction of heat transfer between the nanoparticles and base fluid is basically appropriate for the millimeter- and micrometer-sized particles, which does not consider all of the heat transfer characteristics of the nanoparticles and therefore, cannot predict the heat transfer rates in nano-systems. Clearly, for a more accurate prediction, the surface-interaction effects of nano-systems must be incorporated into the model, which is still a remaining challenge. However, a relatively simple remedy is correcting the above procedure with the help of available experimental results. This was accomplished by introducing a modified heat transfer coefficient between the nanoparticles and the base fluid (Eq. (37)) instead of Eq. (34) into the Eulerian–Eulerian model. The parameter C in Eq. (37) was assumed to be a function of particle concentration and the flow Reynolds number as given by Eq. (38).

$$h_V = C \times \frac{(6k_f \varphi_p \varphi_f \mathrm{Nu}_p)}{d_p^2} \tag{37}$$

$$C = (|5.505 - 9.606 \times 10^{-6}\mathrm{Re}_e^2 + 1.539 \times 10^{-2}\mathrm{Re}_e - 3.973 \times 10^2 \varphi_p|) \times 10^{-9} \tag{38}$$

The coefficient C in Eq. (38) was obtained from the measured data of convective heat transfer coefficients at different flow Reynolds numbers and particle concentrations for the TiO_2/water nanofluid. In addition to the TiO_2/water data, coefficient C is further validated against the available data of Al_2O_3/water [30], as will be discussed later.

Another UDF code in C language was developed for Eq. (37). It was then interpreted and incorporated into the main solver and replaced the original equation. The effect of using the modified model will be further discussed against the experimental measurements.

It should be mentioned that all thermophysical properties of the base fluids employed in the two-phase models are also temperature dependent (Eqs. (12)–(19)); the thermophysical properties of nanoparticles assumed to be temperature independent have been listed in Table 2.

4. Results and discussion

In this section, after evaluating the accuracy of the experimental set-up against the classical correlation, the axial variations of the measured heat transfer coefficients are presented for various concentrations and Reynolds numbers. Next, the results of different numerical models are validated against the experimental measurements, and the most accurate model is determined. Finally, the effects of nanoparticle type and diameter, as well as base fluid type, are investigated via this model.

It should be mentioned that, in all figures, a Reynolds number is defined as $\mathrm{Re}_e = \rho_e U_{in} D_{pipe}/\mu_e$ based on the properties of nanofluids, in which U_{in} is the inlet velocity calculated from the measured flow rate. Therefore, at a given particle concentration, the inlet velocity for all numerical models is identical.

In order to validate the present single-phase numerical model and also to confirm the accuracy and reliability of the present experimental set-up, the average heat transfer coefficient of water flow in the tube is compared with the results of the Shah and London correlation [39]. As shown in Fig. 7, a reasonable agreement between the results obtained from different methods is observed with the maximum deviation of 3%.

Fig. 8 displays the axial variations of the measured heat transfer coefficient for different particle concentrations and Reynolds numbers. The results indicate that the heat transfer coefficient increases with particle concentrations and the Reynolds number,

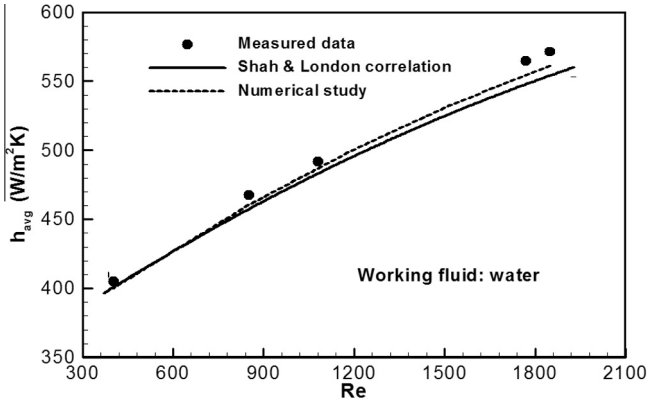

Fig. 7. Comparison of the predicted and measured average heat transfer coefficient against the Shah and London correlation.

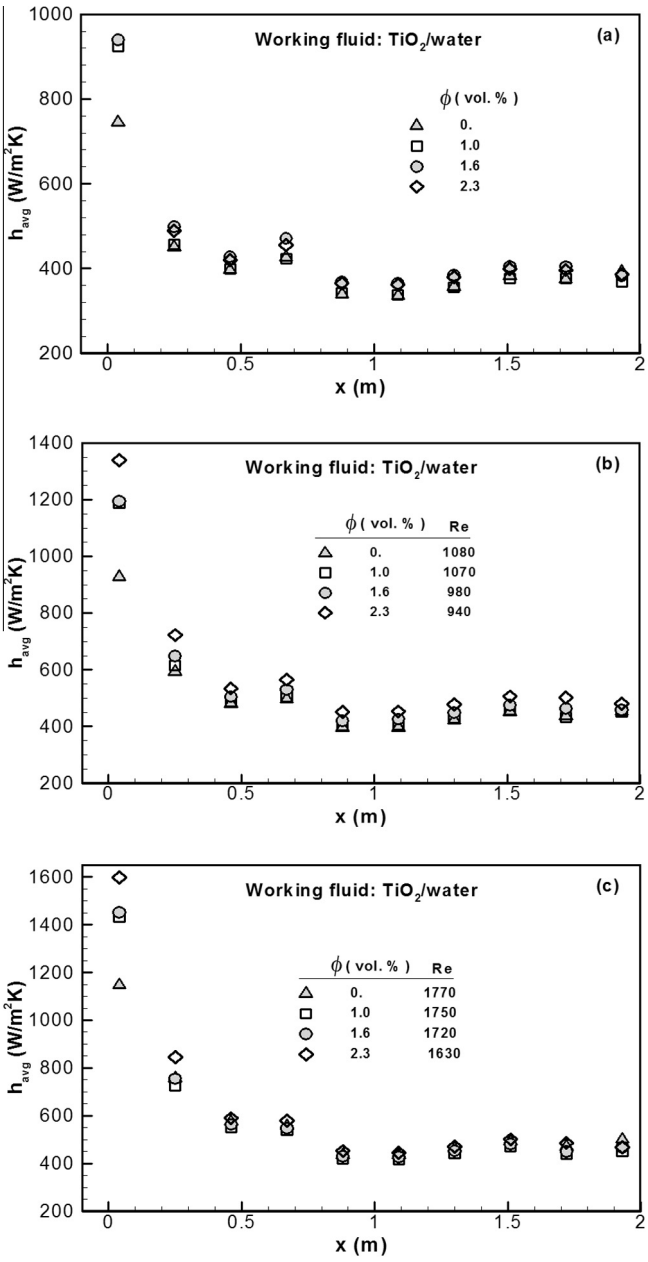

Fig. 8. Variations of local heat transfer coefficient at different nanoparticle concentrations and Reynolds numbers: (a) Re = 370; (b) Re ≈ 1000; (c) Re ≈ 1700.

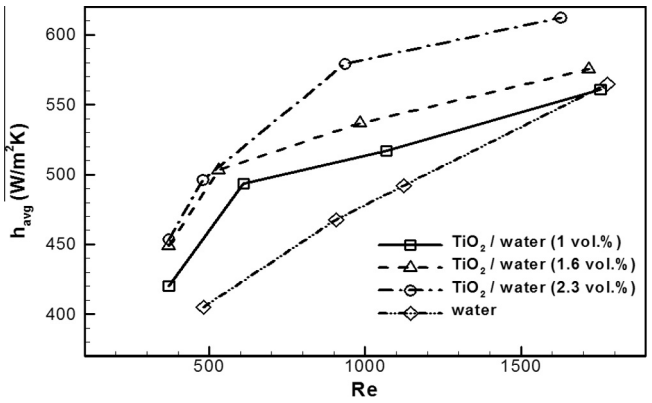

Fig. 9. Variations of the average heat transfer coefficient versus Reynolds number for different particle concentrations of TiO_2/water.

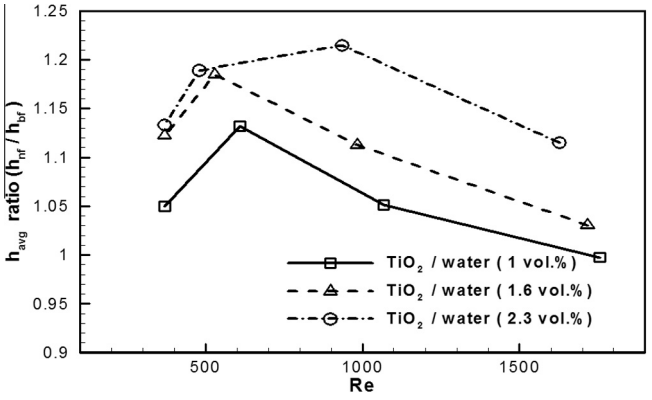

Fig. 10. Variations of the average heat transfer coefficient ratio of nanofluid to water versus Reynolds number for different particle concentrations of TiO_2/water.

where heat transfer enhancements are more noticeable in the thermally developing region.

In order to have a better understanding of the nanofluid effects, the average heat transfer coefficients of the nanofluid and the heat transfer ratio in comparison with that of water is presented in Figs. 9 and 10, respectively. The results prove that the increase in particle concentration enhances the heat transfer characteristics of nanofluids at almost all Reynolds numbers with a non-monotonic fashion. As Fig. 10 shows, in the case of $\varphi = 2.3\%$ and Re = 940, a maximum enhancement of 21% occurs in the average heat transfer coefficients of the nanofluid.

In addition, the results indicate that the ratio of the average heat transfer coefficient of nanofluid to that of the base fluid is maximized at the medial Reynolds numbers. This is due to the fact that the thermal conductivity and viscosity of nanofluids simultaneously increase with an increase of nanoparticle concentration. Therefore, the competition between these two opposing effects determines the amount of heat transfer enhancement for a given Reynolds number.

These remarkable enhancements due to the use of nanofluids cannot be explained by classical mechanisms of heat transfer. Different possible mechanisms have been proposed for the notable convective heat transfer enhancement by nanofluids; one of the most important reasons is the higher thermal conductivity of nanofluids compared to that of base fluids. The Brownian motion of nanoparticles and reduction of the contact angles between nanofluid and pipe surface are among other possible explanations. It has also been suggested [23] that the non-uniform shear rate of nanofluid flow across the tube cross section leading to both viscosity reduction near the tube wall and migration of particles are responsible for the heat transfer enhancement of the nanofluid. This reflects that the increase in thermal conductivity is not the only scenario behind the convective heat transfer enhancement of nanofluids.

This finding demonstrates that the single-phase model still needs to be modified as also indicated by Ebrahimnia-Bajestan et al. [40]. An alternative remedy can be the adaptation of the two-phase models, which have proven to be more accurate [42,43]. In the present study, the common Eulerian–Eulerian two-phase model was employed for simulations as shown in Fig. 11(b). However, as discussed earlier, this model, based on Eq. (34), overestimates the average heat transfer coefficient. The modified model based on Eq. (37), as illustrated in Fig. 11(c), predicts the average heat transfer coefficient more accurately.

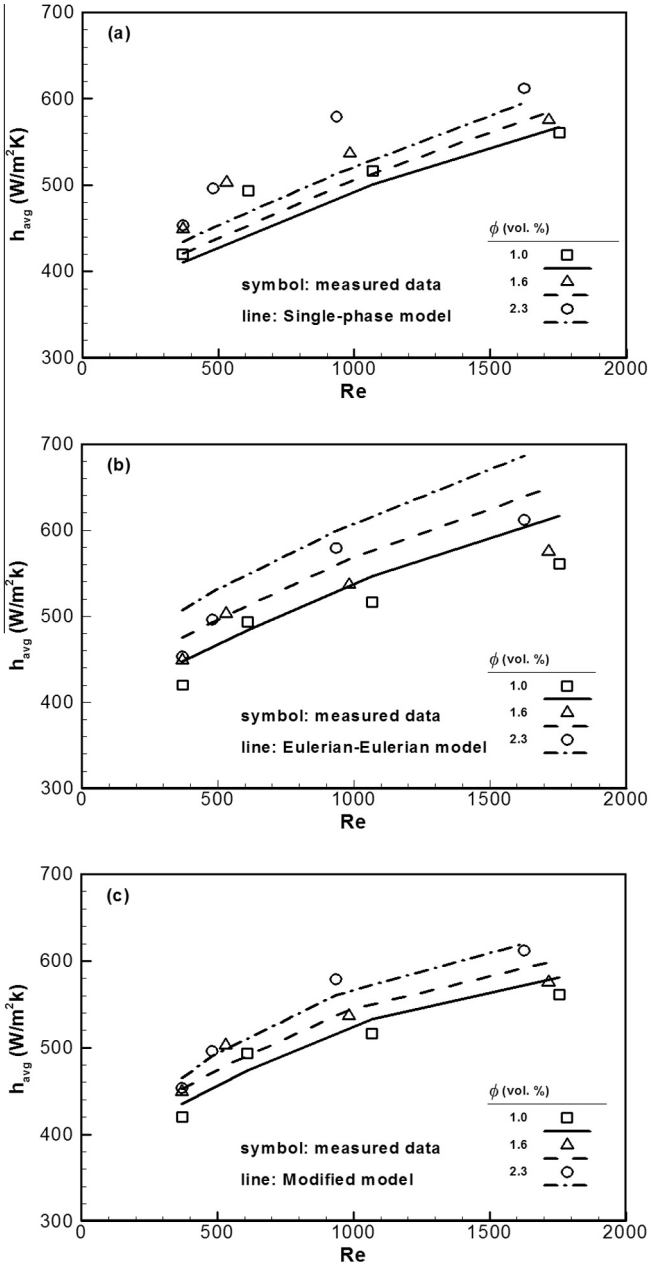

Fig. 11. Comparison of the predicted average heat transfer coefficients against the measured data at different Reynolds numbers and particle concentrations using (a) Single-phase model; (b) Two-phase Eulerian–Eulerian model based on Eq. (34); (c) Two-phase modified model based on Eq. (37).

In addition to the Eulerian–Eulerian model, the mixture model that solves the continuity, momentum, and energy equations for the mixture and the particle concentration equation for the secondary phase can be employed. Various studies have employed this model for the simulation of nanofluids, and the related equations are presented in Fluent 6.3 [59]. In Tables 3 and 4, the resulting average heat transfer coefficients have been compared among the different models discussed so far at various Reynolds numbers and nanoparticle concentrations. As demonstrated, the proposed, modified Eulerian–Eulerian model provides the most accurate results with the maximum deviation of 4.7% compared with the measured data, while this value for the single-phase and two-phase Eulerian–Eulerian model is 11.8% and 12.8%, respectively. It is interesting to note that the mixture and Eulerian–Eulerian models produce almost similar results.

Table 3
Comparison of the different CFD approaches with the measured data at different Reynolds numbers for φ_p = 2.3%.

Re	Error (%)			
	Modified model	Eulerian–Eulerian model	Mixture model	Single-phase model
370	2.48	11.79	11.79	−4.21
480	−1.20	6.46	6.47	−9.23
935	−3.20	3.40	3.41	−11.4
1627	1.30	12.14	12.15	−2.75

Table 4
Comparison of the different CFD approaches with the measured data at different particle concentrations for Re ≈ 1000.

φ_p (%)	Error (%)			
	Modified model	Eulerian–Eulerian model	Mixture model	Single-phase model
1.0	3.10	5.74	5.74	−3.05
1.6	1.23	5.55	5.56	−6.11
2.3	−3.20	3.40	3.41	−11.4

Considering Section 2.2.2, since the uncertainty of average heat transfer coefficient were found to be about 2.8%, the modified Eulerian–Eulerian shows reasonable predictions, while the other models were failed to predict the heat transfer coefficient, accurately. Due to the most accurate predictions, the modified Eulerian–Eulerian model was employed to study the effects of several parameters on convective heat transfer of nanofluids to increase related knowledge for more appropriate application of nanofluids in solar systems.

4.1. Effects of nanoparticle diameter

Fig. 12 shows the effects of particle diameter on the average heat transfer coefficient at different Reynolds numbers and nanoparticle diameters. It shows that increasing particle diameter reduces the average heat transfer coefficient; this effect becomes less significant at higher particle diameters. In addition, the effects of particle concentration are greater for smaller particles and decrease with the increase of particle diameters as shown in Fig. 13, where the variations of the average heat transfer coefficient are plotted versus the particle diameter for different concentrations at Re = 1000. Since the Brownian motions of nanoparticles are considered as the main mechanism of heat transfer in nanofluids, nanoparticles of smaller sizes are associated with stronger

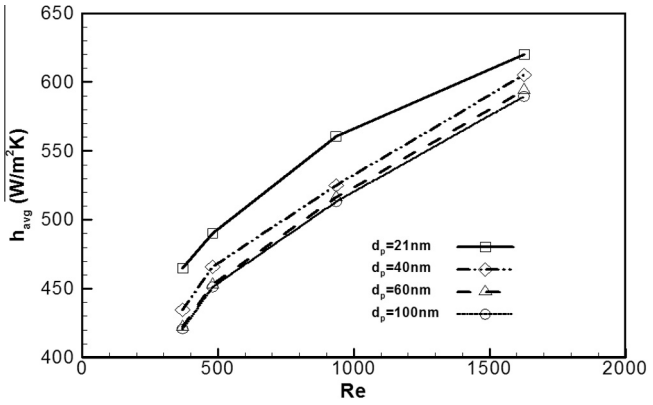

Fig. 12. Variations of the average heat transfer coefficients versus Reynolds number for different particle diameters at φ_p = 2.3% of TiO_2/water nanofluid.

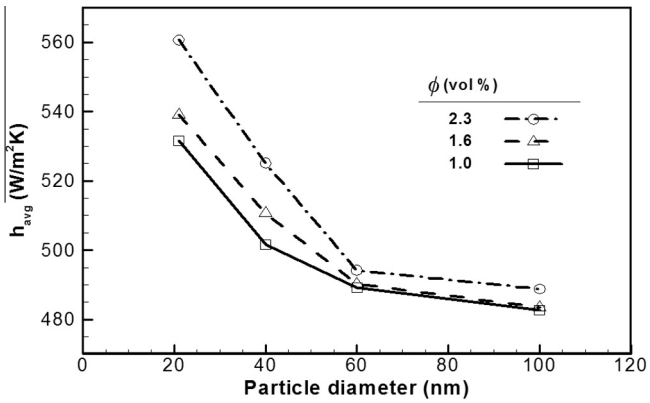

Fig. 13. Variations of the average heat transfer coefficients versus particle diameter for different volume fractions of TiO_2/water nanofluid at Re ≈ 1000.

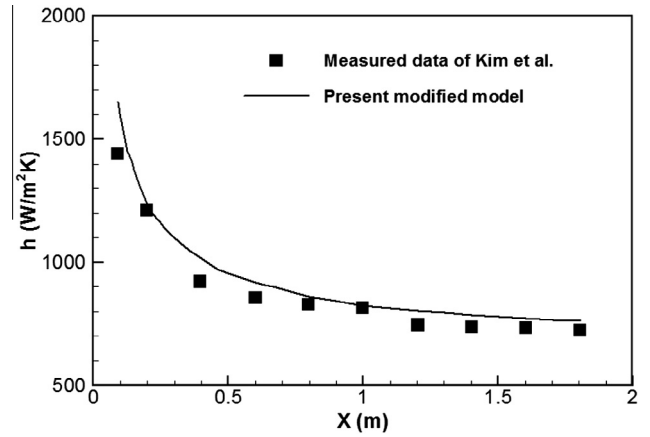

Fig. 14. Comparison of the predicted local heat transfer coefficients with the measured data of 3 vol.% Al_2O_3/water nanofluid at Re = 1460.

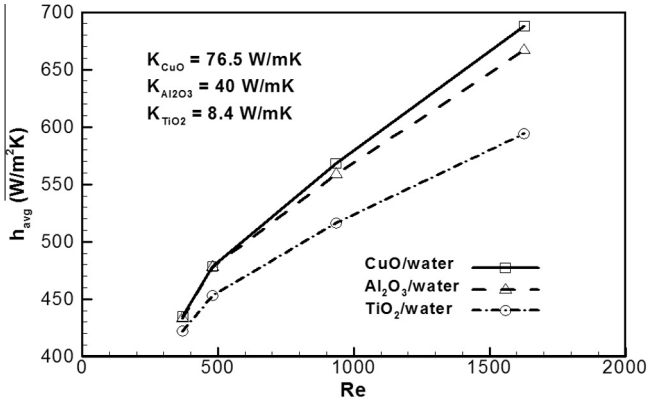

Fig. 15. Variations of the average heat transfer coefficients versus Reynolds number for different particle materials with a given diameter of 60 nm and φ_p = 2.3%.

Brownian motions and enhance the heat transfer characteristics of nanofluids remarkably. Therefore, the employment of smaller nanoparticles is more desirable in solar heat exchangers. However, the process of manufacturing finer particles is more complex and expensive.

4.2. Effects of nanoparticle material

To verify the validity of the presently modified model for other materials, Fig. 14 compares the axial variations of the heat transfer coefficients for the Al_2O_3/water at 3 vol.% nanoparticle volume fraction and Re = 1460 with the measured data of Kim et al. [30]. The results are in good agreement with the measured data, with the deviation of 1.6%. Having reviewed the literature to validate the numerical model for the CuO/water nanofluid, it was found that there was no measured data related to the problem considered in the present study.

Fig. 15 compares the average heat transfer coefficients of the water-based nanofluids for 3 types of materials at different Reynolds numbers. As demonstrated, the heat transfer coefficients are higher for the particles with higher thermal conductivities, which are also enhanced at higher Reynolds numbers.

The obtained data show that nanoparticles with higher thermal conductivities should be employed in solar collectors.

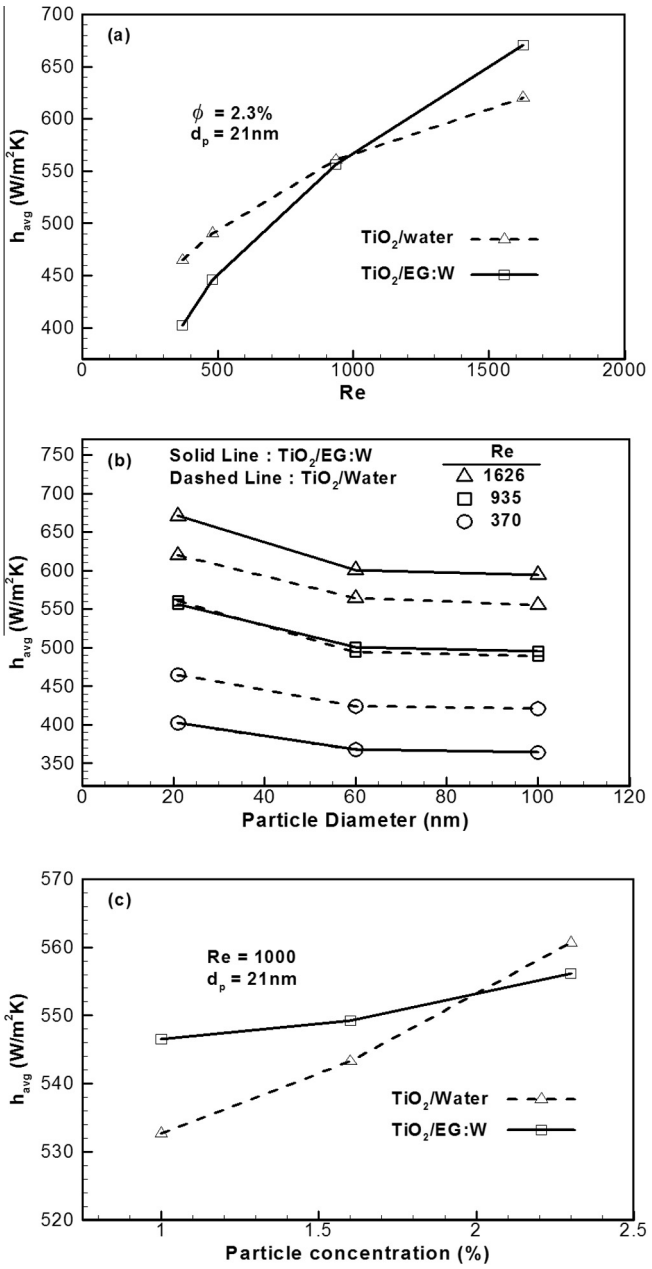

Fig. 16. Effects of basefluid type on the averaged heat transfer coefficients at different (a) Reynolds numbers; (b) particle diameters; and (c) particle concentrations.

It must be noted that the common Eulerian–Eulerian model predicts much larger values for heat transfer coefficients. For example, based on the authors' experience, it predicts a heat transfer coefficient of about 210% larger than the results of the modified model for CuO nanoparticles at the largest Reynolds numbers considered here, which indicates the importance of the appropriate two-phase model selection for heat transfer simulations of nanofluids.

4.3. Effects of base fluid type

In addition to water, a mixture of ethylene glycol to water (EG:W) was also examined as base fluid. This kind of heat transfer fluid is common in cold regions of the world because of its low freezing point, which is effective to protect the solar heaters from freezing. The temperature-dependent properties of this kind of base fluid are presented in Eqs. (16)–(19). Considering these equations, it can be proved that due to the higher viscosity and lower thermal conductivity of EG:W, its heat transfer characteristics is weaker in comparison with that of water. In Fig. 16, the effects of both base fluids on the average heat transfer coefficient are compared at different (a) Reynolds numbers, (b) particle diameters, and (c) particle concentrations. The results indicate that the thermophysical properties of the base fluid strongly affect the nanofluid heat transfer characteristics. It can be concluded that the heat transfer characteristic of EG:W based nanofluid augments with Reynolds number and particle concentration, while it decreases with particle diameter. Considering Figs. 16(a) and (c), it is demonstrated that adding nanoparticles causes the higher enhancement of heat transfer coefficient for the case of EG:W based nanofluid than water based nanofluid at the Reynolds numbers greater than 1000 and particle concentrations lower than 2%, in spite of weaker heat transfer characteristics of EG:W. However at the other ranges the heat transfer coefficients of water based nanofluids are higher. This founding is attributed to the about four times higher viscosity of EG:W than that of water, which also leads to the higher viscosity of EG:W based nanofluid; therefore at low Reynolds numbers and high particle concentrations, where the effect of viscosity is more significant, the EG:W based nanofluid exhibits lower heat transfer coefficient compared with water based nanofluids. Furthermore, as shown in Fig. 16(b), the base fluid type does not significantly change the trend and slope of the heat transfer coefficient curve as a function of particle diameter.

5. Conclusions

The present study investigated a novel method of improving the efficiency of solar systems heat exchangers. For this purpose, it examined laminar convective heat transfer of a TiO_2/water nanofluid flowing through a uniformly heated circular tube both experimentally and numerically. The results indicated that the common single-phase approach, even with measured, temperature-dependent, thermophysical properties, underestimates the convective heat transfer characteristics of nanofluids. Additionally, the common two-phase Eulerian–Eulerian model failed to predict the heat transfer rates accurately. Therefore, as a new solution, the inter-phase heat exchange correlation used in this model was modified, which showed a reasonable agreement with the measured data of the heat transfer coefficient in the case of the TiO_2/water nanofluid.

The study concluded that the heat transfer coefficient of nanofluids is higher than that of the base fluid. Moreover, the Reynolds number and particle concentration, as well as nanoparticle thermal conductivity, caused the convective heat transfer coefficient of nanofluids to increase, whereas particle diameter had an opposite effect on the heat transfer coefficient.

Finally, the maximum enhancement of 21% in average heat transfer coefficient, due to use of nanofluids at low concentration of 2.3 vol.%, indicated the great potential of nanofluids in solar heat exchanger applications. In addition, employing nanofluids having smaller nanoparticles with higher thermal conductivity is recommended for application in solar liquid heating collectors.

Acknowledgment

The financial support of the Ferdowsi University of Mashhad under the grant number of 2/20599 is greatly appreciated. The fourth and fifth author would like to thank the "Research Chair Grant" National Science and Technology Development Agency, the Thailand Research Fund and the National Research University Project for the support.

References

[1] T. Yousefi, F. Veysi, E. Shojaeizadeh, S. Zinadini, An experimental investigation on the effect of Al_2O_3–H_2O nanofluid on the efficiency of flat-plate solar collectors, Renewable Energy 39 (2012) 293–298.
[2] T. Yousefi, E. Shojaeizadeh, F. Veysi, S. Zinadini, An experimental investigation on the effect of pH variation of MWCNT–H_2O nanofluid on the efficiency of a flat-plate solar collector, Sol. Energy 86 (2) (2012) 771–779.
[3] Y. Kameya, K. Hanamura, Enhancement of solar radiation absorption using nanoparticle suspension, Sol. Energy 85 (2) (2011) 299–307.
[4] A. Lenert, E.N. Wang, Optimization of nanofluid volumetric receivers for solar thermal energy conversion, Sol. Energy 86 (1) (2012) 253–265.
[5] Q. He, S. Wang, S. Zeng, Z. Zheng, Experimental investigation on photothermal properties of nanofluids for direct absorption solar thermal energy systems, Energy Convers. Manage. 73 (2013) 150–157.
[6] T. Sokhansefat, A.B. Kasaeian, F. Kowsary, Heat transfer enhancement in parabolic trough collector tube using Al_2O_3/synthetic oil nanofluid, Renew. Sustain. Energy Rev. 33 (2014) 636–644.
[7] O. Mahian, A. Kianifar, S.A. Kalogirou, I. Pop, S. Wongwises, A review of the applications of nanofluids in solar energy, Int. J. Heat Mass Transfer 57 (2) (2013) 582–594.
[8] M. Faizal, R. Saidur, S. Mekhilef, M. Alim, Energy, economic and environmental analysis of metal oxides nanofluid for flat-plate solar collector, Energy Convers. Manage. 76 (2013) 162–168.
[9] Z. Said, R. Saidur, N. Rahim, M. Alim, Analyses of exergy efficiency and pumping power for a conventional flat plate solar collector using SWCNTs based nanofluid, Energy Build. 78 (2014) 1–9.
[10] A.N. Al-Shamani, M.H. Yazdi, M.A. Alghoul, A.M. Abed, M.H. Ruslan, S. Mat, K. Sopian, Nanofluids for improved efficiency in cooling solar collectors – a review, Renew. Sustain. Energy Rev. 38 (2014) 348–367.
[11] A. Kasaeian, A.T. Eshghi, M. Sameti, A review on the applications of nanofluids in solar energy systems, Renew. Sustain. Energy Rev. 43 (2015) 584–598.
[12] P. Mohammad Zadeh, T. Sokhansefat, A.B. Kasaeian, F. Kowsary, A. Akbarzadeh, Hybrid optimization algorithm for thermal analysis in a solar parabolic trough collector based on nanofluid, Energy 82 (2015) 857–864.
[13] M. Sardarabadi, M. Passandideh-Fard, S. Zeinali Heris, Experimental investigation of the effects of silica/water nanofluid on PV/T (Photovoltaic thermal units), Energy 66 (2014) 264–272.
[14] P. Chandrasekaran, M. Cheralathan, V. Kumaresan, R. Velraj, Enhanced heat transfer characteristics of water based copper oxide nanofluid PCM (phase change material) in a spherical capsule during solidification for energy efficient cool thermal storage system, Energy 72 (2014) 636–642.
[15] A.M. Hussein, K.V. Sharma, R.A. Bakar, K. Kadirgama, A review of forced convection heat transfer enhancement and hydrodynamic characteristics of a nanofluid, Renew. Sustain. Energy Rev. 29 (2014) 734–743.
[16] F. Javadi, R. Saidur, M. Kamalisarvestani, Investigating performance improvement of solar collectors by using nanofluids, Renew. Sustain. Energy Rev. 28 (2013) 232–245.
[17] L. Syam, M.K. Sundar Singh, Convective heat transfer and friction factor correlations of nanofluid in a tube and with inserts: a review, Renew. Sustain. Energy Rev. 20 (2013) 23–35.
[18] Q. Li, Y. Xuan, Convective heat transfer and flow characteristics of Cu–water nanofluid, Sci. Chin. Ser. E: Technol. Sci. 45 (4) (2002) 408–416.
[19] D. Wen, Y. Ding, Experimental investigation into convective heat transfer of nanofluids at the entrance region under laminar flow conditions, Int. J. Heat Mass Transfer 47 (24) (2004) 5181–5188.
[20] Y. Ding, H. Alias, D. Wen, R.A. Williams, Heat transfer of aqueous suspensions of carbon nanotubes (CNT nanofluids), Int. J. Heat Mass Transfer 49 (1) (2006) 240–250.
[21] S. Zeinali Heris, S.G. Etemad, M. Nasr Esfahany, Experimental investigation of oxide nanofluids laminar flow convective heat transfer, Int. Commun. Heat Mass Transfer 33 (4) (2006) 529–535.
[22] Y. He, Y. Jin, H. Chen, Y. Ding, D. Cang, H. Lu, Heat transfer and flow behaviour of aqueous suspensions of TiO_2 nanoparticles (nanofluids) flowing upward through a vertical pipe, Int. J. Heat Mass Transfer 50 (11) (2007) 2272–2281.

[23] H. Chen, W. Yang, Y. He, Y. Ding, L. Zhang, C. Tan, A.A. Lapkin, D.V. Bavykin, Heat transfer and flow behaviour of aqueous suspensions of titanate nanotubes (nanofluids), Powder Technol. 183 (1) (2008) 63–72.
[24] K.S. Hwang, S.P. Jang, S.U. Choi, Flow and convective heat transfer characteristics of water-based Al_2O_3 nanofluids in fully developed laminar flow regime, Int. J. Heat Mass Transfer 52 (1) (2009) 193–199.
[25] W. Lai, S. Vinod, P. Phelan, R. Prasher, Convective heat transfer for water-based alumina nanofluids in a single 1.02-mm tube, J. Heat Transfer 131 (11) (2009) 112401.
[26] K. Anoop, T. Sundararajan, S.K. Das, Effect of particle size on the convective heat transfer in nanofluid in the developing region, Int. J. Heat Mass Transfer 52 (9) (2009) 2189–2195.
[27] S.Z. Heris, S.G. Etemad, M.N. Esfahany, Convective heat transfer of a Cu/water nanofluid flowing through a circular tube, Exp. Heat Transfer 22 (4) (2009) 217–227.
[28] U. Rea, T. McKrell, L.-W. Hu, J. Buongiorno, Laminar convective heat transfer and viscous pressure loss of alumina–water and zirconia–water nanofluids, Int. J. Heat Mass Transfer 52 (7) (2009) 2042–2048.
[29] L. Liao, Z.-H. Liu, Forced convective flow drag and heat transfer characteristics of carbon nanotube suspensions in a horizontal small tube, Heat Mass Transfer. 45 (8) (2009) 1129–1136.
[30] D. Kim, Y. Kwon, Y. Cho, C. Li, S. Cheong, Y. Hwang, J. Lee, D. Hong, S. Moon, Convective heat transfer characteristics of nanofluids under laminar and turbulent flow conditions, Curr. Appl. Phys. 9 (2) (2009) e119–e123.
[31] L.G. Asirvatham, B. Raja, D. Mohan Lal, S. Wongwises, Convective heat transfer of nanofluids with correlations, Particuology 9 (6) (2011) 626–631.
[32] M. Chandrasekar, S. Suresh, Experiments to explore the mechanisms of heat transfer in nanocrystalline alumina/water nanofluid under laminar and turbulent flow conditions, Exp. Heat Transfer 24 (3) (2011) 234–256.
[33] S. Ferrouillat, A. Bontemps, J.-P. Ribeiro, J.-A. Gruss, O. Soriano, Hydraulic and heat transfer study of SiO_2/water nanofluids in horizontal tubes with imposed wall temperature boundary conditions, Int. J. Heat Fluid Flow 32 (2) (2011) 424–439.
[34] V. Kumaresan, S. Mohaideen Abdul Khader, S. Karthikeyan, R. Velraj, Convective heat transfer characteristics of CNT nanofluids in a tubular heat exchanger of various lengths for energy efficient cooling/heating system, Int. J. Heat Mass Transfer 60 (2013) 413–421.
[35] H.R. Rayatzadeh, M. Saffar-Avval, M. Mansourkiaei, A. Abbassi, Effects of continuous sonication on laminar convective heat transfer inside a tube using water–TiO_2 nanofluid, Exp. Thermal Fluid Sci. 48 (2013) 8–14.
[36] E. Esmaeilzadeh, H. Almohammadi, S. Nasiri Vatan, A.N. Omrani, Experimental investigation of hydrodynamics and heat transfer characteristics of γ-Al_2O_3/water under laminar flow inside a horizontal tube, Int. J. Therm. Sci. 63 (2013) 31–37.
[37] M.M. Heyhat, F. Kowsary, A.M. Rashidi, M.H. Momenpour, A. Amrollahi, Experimental investigation of laminar convective heat transfer and pressure drop of water-based Al_2O_3 nanofluids in fully developed flow regime, Exp. Thermal Fluid Sci. 44 (2013) 483–489.
[38] J. Wang, J. Zhu, X. Zhang, Y. Chen, Heat transfer and pressure drop of nanofluids containing carbon nanotubes in laminar flows, Exp. Thermal Fluid Sci. 44 (2013) 716–721.
[39] R.K. Shah, A.L. London, Laminar Flow Forced Convection in Ducts, Academic Press, New york, 1978.
[40] E. Ebrahimnia-Bajestan, H. Niazmand, W. Duangthongsuk, S. Wongwises, Numerical investigation of effective parameters in convective heat transfer of nanofluids flowing under a laminar flow regime, Int. J. Heat Mass Transfer 54 (19–20) (2011) 4376–4388.
[41] M. Corcione, M. Cianfrini, A. Quintino, Optimization of laminar pipe flow using nanoparticle liquid suspensions for cooling applications, Appl. Therm. Eng. 50 (1) (2013) 857–867.
[42] M. Keshavarz Moraveji, E. Esmaeili, Comparison between single-phase and two-phases CFD modeling of laminar forced convection flow of nanofluids in a circular tube under constant heat flux, Int. Commun. Heat Mass Transfer 39 (8) (2012) 1297–1302.
[43] R. Lotfi, Y. Saboohi, A.M. Rashidi, Numerical study of forced convective heat transfer of Nanofluids: comparison of different approaches, Int. Commun. Heat Mass Transfer 37 (1) (2010) 74–78.
[44] M.K. Moraveji, R.M. Ardehali, CFD modeling (comparing single and two-phase approaches) on thermal performance of Al_2O_3/water nanofluid in mini-channel heat sink, Int. Commun. Heat Mass Transfer 44 (2013) 157–164.
[45] S. Göktepe, K. Atalık, H. Ertürk, Comparison of single and two-phase models for nanofluid convection at the entrance of a uniformly heated tube, Int. J. Therm. Sci. 80 (2014) 83–92.
[46] M. Haghshenas Fard, M.N. Esfahany, M.R. Talaie, Numerical study of convective heat transfer of nanofluids in a circular tube two-phase model versus single-phase model, Int. Commun. Heat Mass Transfer 37 (1) (2010) 91–97.
[47] M. Kalteh, A. Abbassi, M. Saffar-Avval, J. Harting, Eulerian–Eulerian two-phase numerical simulation of nanofluid laminar forced convection in a microchannel, Int. J. Heat Fluid Flow 32 (1) (2011) 107–116.
[48] R. Mokhtari Moghari, A. Akbarinia, M. Shariat, F. Talebi, R. Laur, Two phase mixed convection Al_2O_3–water nanofluid flow in an annulus, Int. J. Multiphase Flow 37 (6) (2011) 585–595.
[49] V. Bianco, F. Chiacchio, O. Manca, S. Nardini, Numerical investigation of nanofluids forced convection in circular tubes, Appl. Therm. Eng. 29 (17–18) (2009) 3632–3642.
[50] Y.-T. Yang, Y.-H. Wang, P.-K. Tseng, Numerical optimization of heat transfer enhancement in a wavy channel using nanofluids, Int. Commun. Heat Mass Transfer 51 (2014) 9–17.
[51] M. Nuim, M.J. Labib, H. Nine, H. Afrianto, H. Chung Jeong, Numerical investigation on effect of base fluids and hybrid nanofluid in forced convective heat transfer, Int. J. Therm. Sci. 71 (2013) 163–171.
[52] M. Kalteh, A. Abbassi, M. Saffar-Avval, A. Frijns, A. Darhuber, J. Harting, Experimental and numerical investigation of nanofluid forced convection inside a wide microchannel heat sink, Appl. Therm. Eng. 36 (2012) 260–268.
[53] B.C. Pak, Y.I. Cho, Hydrodynamic and heat transfer study of dispersed fluids with submicron metallic oxide particles, Exp. Heat Transfer 11 (2) (1998) 151–170.
[54] G.A. Longo, C. Zilio, Experimental measurement of thermophysical properties of oxide–water nano-fluids down to ice-point, Exp. Thermal Fluid Sci. 35 (7) (2011) 1313–1324.
[55] T. Yiamsawas, O. Mahian, A.S. Dalkilic, S. Kaewnai, S. Wongwises, Experimental studies on the viscosity of TiO_2 and Al_2O_3 nanoparticles suspended in a mixture of ethylene glycol and water for high temperature applications, Appl. Energy 111 (2013) 40–45.
[56] W. Duangthongsuk, S. Wongwises, Measurement of temperature-dependent thermal conductivity and viscosity of TiO_2–water nanofluids, Exp. Thermal Fluid Sci. 33 (4) (2009) 706–714.
[57] J. Koo, C. Kleinstreuer, Laminar nanofluid flow in microheat-sinks, Int. J. Heat Mass Transfer 48 (13) (2005) 2652–2661.
[58] R. American Society of Heating, A.-C. Engineers, ASHRAE Handbook: Fundamentals, ASHRAE, 2001.
[59] Fluent 6.3 User's Guide, in, Fluent Inc, Lebanon, New Hampshire, 2006.
[60] L. Schiller, Z. Naumann, A drag coefficient correlation, Z. Ver Deutsch. Ing. 77 (1935) 318–320.
[61] W. Ranz, W. Marshall, Evaporation from drops, Chem. Eng. Prog. 48 (3) (1952) 141–146.